

Decomposition and Synthesis of High-Order Compensated Inductive Power Transfer Systems for Improved Output Controllability

Rong He, *Student Member, IEEE*, Peng Zhao, *Student Member, IEEE*, Minfan Fu^{ib}, *Member, IEEE*, Yu Liu, *Member, IEEE*, Haoyu Wang^{ib}, *Senior Member, IEEE*, and Junrui Liang^{ib}, *Member, IEEE*

Abstract—High-order compensation provides more design freedom for inductive power transfer systems and can help improve output voltage/current controllability. This paper develops a simplified decomposition and synthesis method for high-order-compensated inductive power transfer systems. It can achieve load-independent (LI) output under coupling variation, and easily fulfill the various charging requirements, such as constant voltage or constant current. The coupling independent resonance is ensured by using the induced source model, and the whole resonant tank is effectively decomposed as three parts. The power transfer characteristics are discussed for each part, and the requirements for LI output and zero phase angle (ZPA) operation are combined to generate the compensation candidates for both sides. Two families of topologies are synthesized for four kinds of conversions, i.e., voltage to voltage, voltage to current, current to voltage, and current to current. Meanwhile, the proposed method dramatically simplifies the evaluation for the influence of the coil equivalent series resistors on the transfer function and efficiency. These resistor-caused effects are quite different for two families of topologies. Finally, a 6.78-MHz system with 10-W output is designed to verify the difference between two-family topologies.

Index Terms—Coupling-independent (CI) resonance, decomposition and synthesis, high-order compensation, inductive power transfer, load-independent (LI) output, zero phase angle (ZPA) operation.

I. INTRODUCTION

INDUCTIVE power transfer (IPT) has been widely applied to charge wearable devices, cellphones, and electric vehicles [1], [2]. Usually, each specific application has its own demands on the power level, efficiency, size, and spatial freedom, which would finally determine the suitable resonant frequency, topology, system configuration, and control scheme [3]–[5]. For all these IPT systems, the selection and

design of proper compensation is a common issue. About 15 years ago, the group from the University of Auckland proposed four basic compensations, i.e., series–series (SS), parallel–series (PS), series–parallel (SP), and parallel–parallel (PP), to boost the power transfer capability and achieve zero phase angle (ZPA) operation [6], [7]. Since then, many IPT systems have been developed. However, most of the reported systems have to use complicated switch-mode circuits to maintain good controllability for various objectives, such as constant output voltage, dynamic impedance matching, and optimal efficiency tracking [8]–[10]. Recently, the four basic compensations are also explored for load-independent (LI) output voltage or current to improve the controllability and simplify the system configuration [11]–[14]. However, most systems cannot keep LI output and ZPA operation when the coupling varies. Therefore, it is challenging to achieve various objectives with simple circuits and control scheme.

In theory, the four basic compensations are difficult to meet various demands simultaneously because of the limited design freedom. Therefore, it is possible to employ high-order compensations to overcome this issue, and then additional objectives can be fulfilled [15]–[17]. For example, the *LC* compensation offers an input-voltage-controlled current to drive the transmitter (TX) coil, and then power demands of each receiver (RX) are effectively decoupled [15]. The *LCC* compensation is proposed in [16] for zero-current-switching (ZCS). The double-sided *LCC* compensation can achieve the LI output, zero-voltage-switching (ZVS), and ZPA operation simultaneously [17]. When the compensation order increases, the possible combination of resonant components would dramatically increase as well. Several papers are devoted to the design and selection of proper compensations. In [18], the basic circuit networks for LI output are summarized and used to explain the existing compensations. Based on these findings, several rules have been abstracted to synthesize high-order compensations by representing the coupling coils as a T-type circuit or classical transformer [19], [20]. However, this kind of coil modeling is hard to analyze the coupling variation cases. This issue is effectively avoided in [21] by using the induced source model, i.e., modeling the coils as the

Manuscript received February 20, 2019; revised May 16, 2019; accepted June 16, 2019. Date of publication August 2, 2019; date of current version November 5, 2019. This work was supported in part by the Shanghai Sailing Program under Grant 19YF1433700 and in part by the Shanghai Program for Professor of Special Appointment (Eastern Scholar, Youth). (*Corresponding author: Minfan Fu.*)

The authors are with the School of Information Science and Technology, ShanghaiTech University, Shanghai 201210, China (e-mail: fumf@shanghaitech.edu.cn).

Color versions of one or more of the figures in this article are available online at <http://ieeexplore.ieee.org>.

Digital Object Identifier 10.1109/TMTT.2019.2929143

combination of self-inductance and induced voltage source. Since the self-inductance is used for resonance, the derived frequencies for LI output and ZPA operation can be naturally coupling independent (CI).

This paper proposes a novel perspective to simplify the decomposition and synthesis for high-order-compensated IPT systems. All kinds of LI conversions, i.e., voltage to voltage (V2V), voltage to current (V2I), current to voltage (I2V), and current to current (I2I) are discussed based on the induced source model, which can naturally help analyze the CI resonance. The self-inductance of the TX coil is aborted by the TX compensation to form a resonant tank, so as for the RX side. The whole resonant tank can then be decomposed into three parts, i.e., a TX tank, a pair of induced voltage sources, and an RX tank. This system decomposition dramatically simplifies the system analysis and each part can be designed in a decoupled manner. Since the transfer functions of the induced voltage source are well known, the main challenge becomes how to develop high-order resonant tank candidates (for both sides) that enable LI output and ZPA operation. In order to solve this challenge, many well-developed methods for conventional high-order resonant converters can be modified and applied in this paper [22]. The basic requirements for LI output and ZPA operation are gradually applied to generate all the tank candidates. To the best of author's knowledge, it is the first time to propose a rule to generate all the tank candidates (up to fourth order) for all kinds of conversions, which would finally help synthesize the high-order IPT topology. Finally, two families of fundamental topologies for all kinds of conversions are found, and two example topologies for V2V conversion are studied and compared.

II. COUPLING-INDEPENDENT (CI) RESONANCE

A. Limitation of Transformer Model or T Model

A typical IPT system is shown in Fig. 1. The power is coupled from the TX coil (L_{tx}) to the RX coil (L_{rx}). Since the mutual inductance (M) is small, both TX and RX compensations are necessary to boost the power transfer capability. In this paper, high-order compensations are employed to improve the system controllability. In practice, the output current or voltage should be regulated to meet specific power demand and port requirements. When a resonant tank is able to provide LI transfer function under coupling variation, the output regulation complexity could be significantly reduced. For example, if the resonant tank can offer LI V2V gain and its associated operation frequency will not shift under coupling variation (i.e., coupling-independent resonance), it means the input voltage v_{in} can be used to directly control the output voltage v_o . Therefore, this paper is devoted to the decomposition and synthesis of high-order compensation with LI output, CI resonance, and ZPA operation.

In order to analyze the resonant tank, a straightforward and convenient method is to apply the classical transformer model for the coupling coils, and then an IPT system can be treated as an entity, which is actually a special isolated resonant converter. Fig. 1 shows the transformer model, in which the magnetizing inductance L_m , the leakage inductance L_l , and

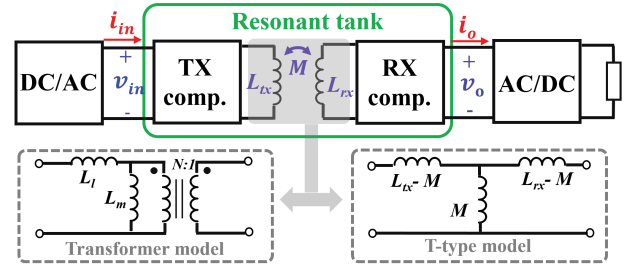


Fig. 1. IPT system block diagram.

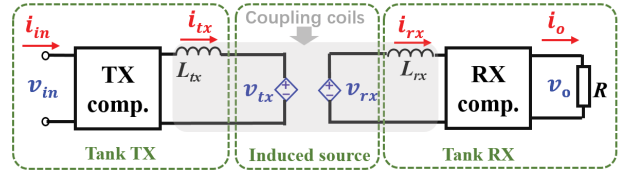


Fig. 2. IPT system decomposition.

the equivalent turn ratio N (not the real one) can be represented in terms of the self-inductance and mutual inductance (i.e., L_{tx} , L_{rx} , and M)

$$\begin{aligned} L_m &= M^2 / L_{rx} \\ L_l &= L_{tx} - M^2 / L_{rx} \\ N &= M / L_{rx}. \end{aligned} \quad (1)$$

It shows all the transformer parameters are actually coupling-dependent. Once these varied inductances join the resonance, the resonance frequency will shift when the coil position varies. The T-type model has similar issues (refer to Fig. 1). Therefore, all the compensation analysis based on these models (including coupling-dependent inductance) naturally face more challenges [19], [20].

B. System Decomposition

In order to achieve CI resonance, the resonant components have to be coupling-independent. Since fixed compensation networks (i.e., lumped capacitors or inductors with fixed value) are usually used, the only uncertain components come from the coupling coils (refer to Fig. 1). To avoid this issue, the coupling coils should be modeled with fixed components [21]. Therefore, as shown in the gray part of Fig. 2, the coupling coils are represented by the well-known induced source model, i.e., a combination of the two self-inductances (L_{tx} and L_{rx}) and a pair of induced voltage sources (v_{tx} and v_{rx}). i_{tx} and i_{rx} are the current of L_{tx} and L_{rx} . It has

$$\begin{aligned} v_{tx} &= -j\omega_s i_{rx} M \\ v_{rx} &= j\omega_s i_{tx} M \end{aligned} \quad (2)$$

where ω_s is the angular switching frequency.

Using the induced source model, a classical system decomposition approach is proposed in Fig. 2, and the whole resonant tank is viewed as a cascaded connection of three parts, i.e., Tank TX, the induced source part, and Tank RX. L_{tx} and L_{rx} are in series with TX/RX compensations to form

Tank TX/RX, respectively. The induced source part only includes v_{tx} and v_{rx} . For Tank TX, v_{in} and i_{in} are the input voltage and current. Similarly, v_o and i_o are the output voltage and current of Tank RX. In this paper, Tank TX and Tank RX can be analyzed individually for a target resonant frequency, and then various objectives (like loading-independent output and ZPA operation) can be achieved by proper selection and design of resonant tanks. Since all the resonant components are fixed, the proposed decomposition method can naturally help to synthesize all coupling-independent IPT topologies.

III. LOAD-INDEPENDENT OUTPUT

A. Transfer Function of the Induced Source Part

The LI output (voltage or current) is preferred for an IPT system due to its good controllability. In this paper, G is used to define the input to output transfer function, and the subscript is used to denote the conversion type (like V2V) and different parts of the IPT system. For example, $G_{coil,vi}$ means the transfer function from v_{tx} to i_{rx} in Fig. 2. Since the system is a cascaded connection of three parts, the overall transfer function is the product of the gain of each sub part. According to (2), the induced source part can naturally provide LI transfer function, that is,

$$\begin{aligned} G_{coil,iv} &= \frac{v_{rx}}{i_{tx}} = j\omega_s M \\ G_{coil,vi} &= \frac{i_{rx}}{v_{tx}} = -\frac{1}{j\omega_s M}. \end{aligned} \quad (3)$$

It shows there are only two approaches to achieve LI voltage/current transfer. Therefore, two families of IPT topologies are defined. If an IPT topology is synthesized based on LI $G_{coil,iv}$, it belongs to Family A, and LI $G_{coil,vi}$ is used to generate the topologies of Family B.

B. Basic LI Resonant Networks

Given LI conversions for the induced source part, the next objective is to find the suitable LI resonant tanks for Tank TX/RX. Usually, the LI output happens at a certain frequency for a given resonant tank. For example, a LLC resonant converter provides a LI output voltage when working at its series resonant frequency. Many studies on high-order resonant converters can help to find proper candidates. The basic network with LI output has been discussed in [18] and shown in Fig. 3. The impedance requirements and the transfer function are summarized in Table I. For example, a LC circuit provides LI G_{vi} , which can be easily explained by the Norton's theory [refer to Fig. 3(c)]. Note that $Z_2 = \infty$ in Fig. 3(a) also provides LI G_{vv} , and $Z_1 = Z_3 = \infty$ in Fig. 3(b) offers LI G_{ii} . These fundamental blocks are used to generate high-order network with LI transfer functions.

In [20], the overall IPT resonant tank can be viewed as a cascaded connection of these basic LI networks. As shown in Fig. 4, the coupling coils are usually modeled as a T-type network. Although this modeling method can help explain the existing high-order IPT systems, it is inconvenient to analyze the coupling-independent resonance. For example, Zhang *et al.* [11] and Costanzo *et al.* [14] used the SS compensation for

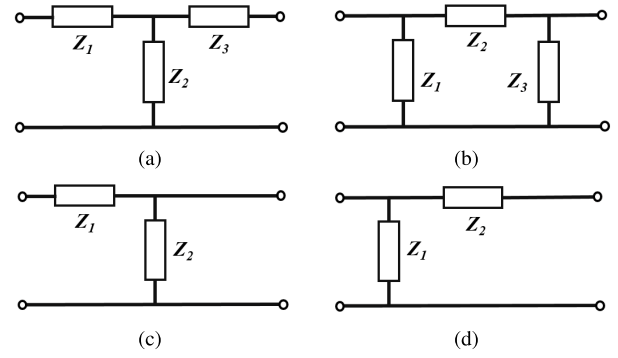


Fig. 3. Basic circuit network with LI output. (a) LI G_{vv} . (b) LI G_{ii} . (c) LI G_{vi} . (d) LI G_{iv} .

TABLE I
IMPEDANCE REQUIREMENT FOR LI TRANSFER FUNCTIONS

Basic network	Impedance requirement	LI transfer function
Fig. 3 (a)	$Z_1 Z_2 + Z_2 Z_3 + Z_3 Z_1 = 0$	$G_{vv} = Z_2 / (Z_1 + Z_2)$
Fig. 3 (b)	$Z_1 + Z_2 + Z_3 = 0$	$G_{ii} = -Z_1 / Z_3$
Fig. 3 (c)	$Z_1 + Z_2 = 0$	$G_{vi} = 1 / Z_1$
Fig. 3 (d)	$Z_1 + Z_2 = 0$	$G_{iv} = Z_1$

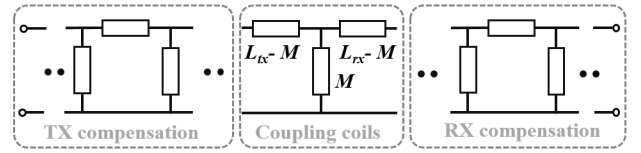


Fig. 4. Synthesis method in [20].

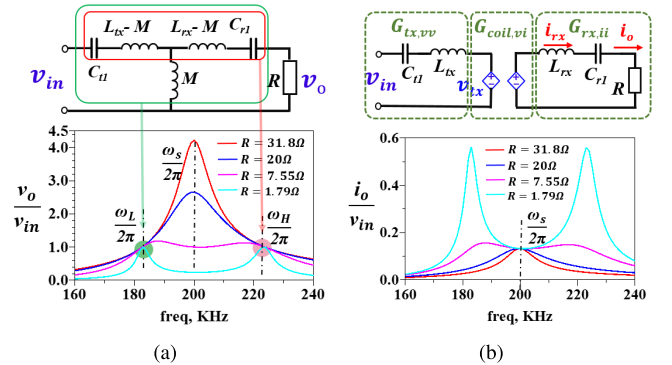


Fig. 5. SS compensation for LI output. (a) Coupling-dependent G_{vv} . (b) Coupling-independent G_{vi} .

LI output voltage. Two LI resonant frequencies (ω_H and ω_L) are analytically derived and shown in Fig. 5(a). Using the synthesis approach of [20], the corresponding resonant networks for each LI resonant frequency can be easily identified, i.e., the resonance of the red block used to derive ω_H and the resonance of the green part used to derive ω_L . It is obvious that both ω_H and ω_L are coupling-dependent because of the varied M .

The SS compensation is also used for LI G_{vi} as shown in Fig. 5(b) [13]. The proposed decomposition in this paper can be used to easily analyze the resonance condition. For Tank TX, the resonance between L_{tx} and C_{t1} makes v_{tx}

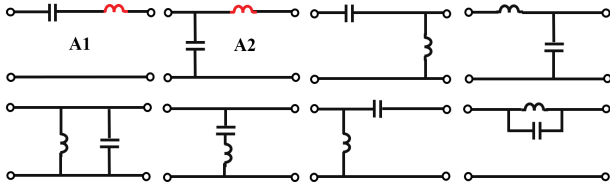


Fig. 6. Second-order resonant tanks (the red inductor means the coupling coil).

clamped by v_{in} , i.e., LI $G_{tx,vv}$, which further leads to a clamped i_{rx} , i.e., LI $G_{coil,vi}$ [refer to (3)]. Finally, Tank RX is also a series LC branch with LI $G_{rx,ii}$. Therefore, the overall voltage to current transfer function is a product form, i.e., $G_{vi} = G_{tx,vv}G_{coil,vi}G_{rx,ii}$. Instead of analyzing the whole tank, this paper chooses to analyze the LI transfer function of each parts, based on which the derived resonance frequency is naturally CI.

C. Candidate Resonant Tanks for Topology Synthesis

The proposed decomposition method can not only better explain the existing IPT topologies, but also provide an effective way for topology synthesis. It helps the IPT system to have LI output capability at CI resonant frequency. Due to the source or load type (i.e., voltage or current), there are totally four types of transfer functions (i.e., G_{vv} , G_{ii} , G_{vi} , and G_{iv}). For each type of conversion, there are two effective ways to utilize the coupling coils, i.e., $G_{coil,vi}$ and $G_{coil,iv}$, which are used to define two-family topologies. For example, the overall gain for V2V conversion (G_{vv}) can be decomposed either as $G_{vv} = G_{tx,vv}G_{coil,vi}G_{rx,iv}$ (belonging to Family A) or as $G_{vv} = G_{tx,vi}G_{coil,iv}G_{rx,vv}$ (belonging to Family B). Therefore, this paper needs to develop a candidate pool for Tank TX and Tank RX for all kinds of conversions (i.e., V2V, V2I, I2V, and I2I).

The study of high-order resonant converter is not new, and there is a continuous effort on topology synthesis for the traditional resonant converter. The major difference between the traditional resonant converter and the IPT system is the varied coupling. In this paper, the induced source and the fixed self-inductance of the coupling coils are treated separately, and it helps to directly utilize the analysis methods of the traditional high-order resonant converter. Up until now, there is no paper to summarize all the possible high-order compensated IPT systems for various conversions, i.e., V2V, V2I, I2V, and I2I.

Due to the symmetry, Tank TX and RX actually share the same candidate pool. For example, a candidate for Tank TX with LI $G_{tx,vi}$ can directly serve as Tank RX for LI $G_{rx,iv}$. The following discussion only needs to focus on the TX side. As shown in Fig. 2, all the tank candidates should ensure there is at least a series inductor (used as the L_{tx}) at the output terminal. Therefore, the simplest resonant tank with LI output capability is to combine a series or shunt capacitor with L_{tx} . Fig. 6 shows all the second-order tanks. Based on the conclusion of Fig. 3 and Table I, only Tank A1 and Tank A2 (including L_{tx} , the red inductor) can serve as the candidates with LI output capability.

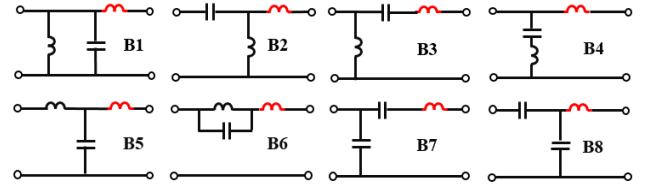


Fig. 7. Third-order tank candidates with LI output capability (the red inductor means the coupling coil).

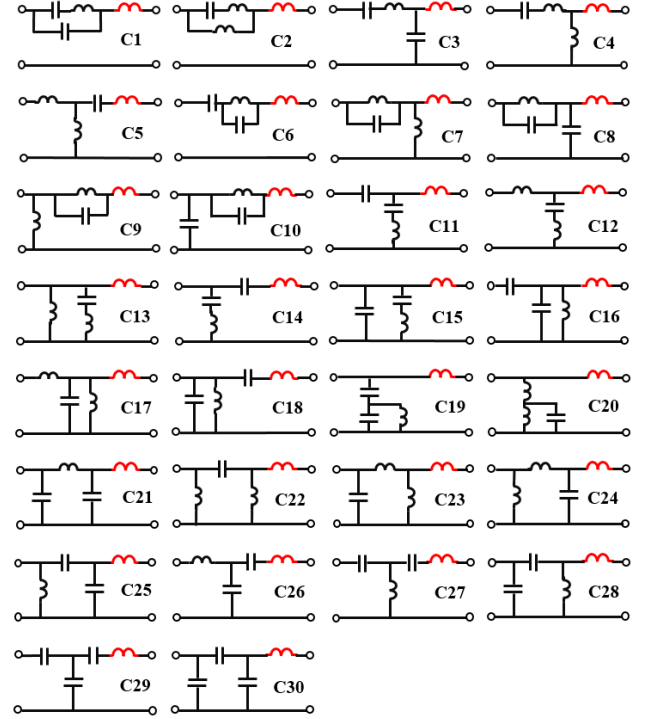


Fig. 8. Fourth-order tank candidates with LI output capability (the red inductor means the coupling coil).

The third-order tank candidates are generated based on the second-order tanks in Fig. 6, i.e., adding a series L_{tx} to the output port. Note that Tank A1 and A2 should not be used because two inductors will merge to form a lower-order tank at the output port. In Fig. 7, six tanks (i.e., Tanks B1–B6) are generated based on this principle. Tanks B7 and B8 are created based on two-capacitor networks, which are not included in Fig. 6. There are totally 36 third-order resonant tanks, among which only 28 tanks (excluding those in Fig. 7) can be used to generate the fourth-order candidates (refer to Tanks C1–C28 in Fig. 8). Tanks C29 and C30 are generated by three-capacitor networks. The proposed candidate generation approach is valid for even higher-order tanks, and more than one hundred candidates can be generated for fifth-order tanks. Presently, the benefit for further increasing the tank order is not obvious, and this paper would focus on the proposed tanks up to fourth-order.

D. Candidate Tank Classification

The LI transfer functions of the proposed candidates are determined based on Fig. 3. For example, if a candidate

$G_{Lx,vv}$	A1, B2, B3, B5, B6, B7, B8, C1, C2, C3, C4, C5, C6, C7, C8, C9, C10, C11, C12, C14, C16, C17, C18, C21, C22, C24, C25, C26, C27, C28, C29, C30
$G_{Lx,vi}$	B2, B5, C3, C4, C7, C8, C11, C12, C16, C17, C21, C22, C24, C26, C27, C28
$G_{Lx,iv}$	A2, B1, B3, B4, B5, B7, B8, C3, C5, C8, C9, C10, C11, C12, C13, C14, C15, C16, C17, C18, C19, C20, C21, C22, C23, C24, C25, C26, C27, C28, C29, C30
$G_{Lx,ii}$	A1, B1, B6, C21, C22, C23, C24, C25, C28
$G_{rx,ii}$	

Fig. 9. Tank candidates with LI output and CI resonance.

tank can be viewed as the T-type network and meets the requirement of Table I, it will offer LI G_{vv} . Similar rules are also valid for the other three kinds of conversions. Finally, Fig. 9 classifies the candidate tanks based on the conversion type. These tanks are able to explain most of the existing well-known IPT topologies. For example, the SS compensation can offer LI G_{vi} , which is a combination of Tank A1 (as Tank TX, enabling LI $G_{Lx,vv}$), the induced voltage (enabling LI $G_{coil,vi}$), and Tank A1 (reversely used as Tank RX, enabling LI $G_{Lx,ii}$); the double-sided LCC compensation offers LI G_{vi} based on the cascaded connection of Tank C26 ($G_{Lx,vi}$), induced source (G_{iv}), and reversed Tank C26 ($G_{Lx,vi}$).

IV. ZERO PHASE ANGLE OPERATION

Given the candidate pool, many new IPT topologies can be synthesized with LI output and CI resonance. However, the IPT system still needs to consider other significant objectives. Actually, at the very beginning of IPT research, the four basic compensations are developed only for sufficient power transfer. For example, the RX compensation is used to maximize the output capability, i.e., fully utilizing the induced voltage of the RX side, v_{rx} , and the TX compensation is used to achieve ZPA operation for minimum VA rating. The reduced circulating energy is helpful to lower the device stress and the conduction losses, which is particularly important for high-power applications. Therefore, it is still meaningful to achieve the ZPA operation, which can help narrow down the available candidates in Table I. By reviewing the four basic compensations, the RX compensation is either a shunt capacitor or series capacitor, whose capacitance is fixed and only determined by L_{rx} . However, the TX compensation capacitance is quite different, only the SS can achieve coupling and loading-independent compensation. Since the fixed compensation network is preferred, this part focuses on how to select and design the fixed compensation network with ZPA operation. If a half- or full-bridge inverter is used, ZVS or ZCS may be required. Then, the resonant tank with ZPA operation should be slightly modified to have an inductive Z_{in} (ZVS) or capacitive Z_{in} (ZCS). These considerations have been discussed in many papers and will not be elaborated here [16], [17].

Fig. 10 shows the port impedance of the IPT system. Z_{in} , Z_{ref} , Z_{rx} , and R are the input impedance of Tank TX, the reflected impedance, the input impedance of Tank RX, and final load resistance. r_{tx} and r_{rx} are the ESRs of L_{tx} and L_{rx} . In this paper, the coils' ESRs are separated from the self-inductance and equivalently viewed as the source internal resistance. η_{tx} , η_{rx} , and η_{coil} are the efficiency of the TX

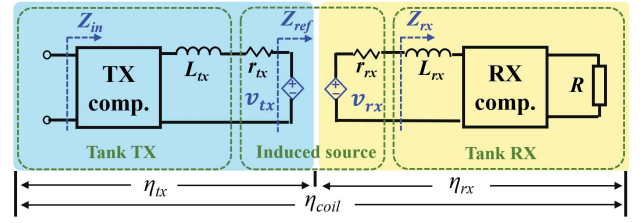


Fig. 10. Port impedance.

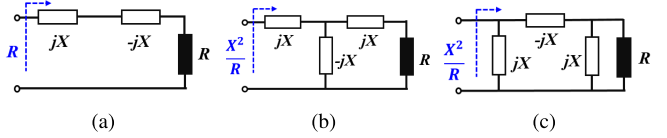


Fig. 11. Basic resistance transformation networks. (a) Series network with noninverted input resistance. (b) T-type network with inverted input resistance. (c) Pi-type network with inverted input resistance.

$G_{Lx,vv}$ or $G_{rx,vv}$:	A1, B3, B6, B7, C1, C2, C6,
$G_{Lx,vi}$ or $G_{rx,iv}$:	B5, C3, C8, C12, C17, C26, C27
$G_{Lx,iv}$ or $G_{rx,vi}$:	B5, C3, C8, C12, C17, C26, C27
$G_{Lx,ii}$ or $G_{rx,ii}$:	A1, B6

Fig. 12. Tank candidates for ZPA operation.

side, the RX side, and the whole tank, respectively. In order to achieve ZPA, Tank TX should be able to compensate the reactive part of Z_{ref} , that is,

$$Z_{ref} = \frac{\omega^2 k^2 L_{tx} L_{rx}}{Z_{rx} + r_{rx}} \quad (4)$$

where k is the coupling coefficient and equals to $M/\sqrt{L_{tx}L_{rx}}$. A fixed TX compensation requires a resistive Z_{ref} , otherwise Z_{ref} will include a coupling-dependent reactive part and can only be fully compensated by a dynamic impedance matching network. Based on this concern, Z_{rx} has to be purely resistive as well, and then a resistive Z_{ref} is obtained based on (4).

At the RX side, Z_{rx} is determined by the load R and Tank RX. In order to have a resistive Z_{rx} at the resonant frequency, Tank RX should be a resistance transformation network without introducing any reactive components. Three simplest resistance transformation networks are given as shown in Fig. 11. A series branch (i.e., a LC tank) gives a noninverted input resistance, while a T-type or Pi-type network gives an inverted input resistance. Higher-order resistance transformation networks can be built based on these basic blocks. Therefore, the network requirement for ZPA operation actually helps narrow down the candidate tanks as shown in Fig. 12.

Based on the proposed synthesis method, a large number of topologies can be generated for four basic conversions. For each type of conversion, two families of topologies with lowest order are given in Fig. 13. The coupling coils can offer LI $G_{coil,iv}$ and $G_{coil,vi}$ [refer to (3)]. In this paper, $G_{coil,iv}$ is used to generate Family-A topologies, while $G_{coil,vi}$ can generate Family-B topologies. Among these topologies, only the clamped voltage/current is denoted. For example, Tank TX of VVA is designed for LI $G_{Lx,vi}$ (from v_{in} to i_{tx}), and Tank RX is responsible for LI $G_{Lx,vv}$ (from v_{rx} to v_o).

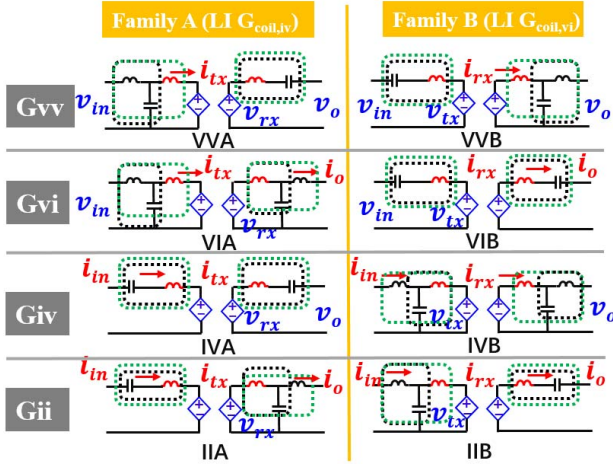


Fig. 13. Fundamental IPT topologies enabling CI resonance, LI output, and ZPA operation.

The circuit components within the black block are designed for the LI transfer function, and Table I should be applied. Meanwhile, the circuit within the green block is responsible for the resistance transformation, and Fig. 11 should be used. These basic requirements are combined to design the component value. The proposed synthesis offers a very simple and straightforward approach to get all possible high-order compensation with desirable controllability. The LI frequency can be easily derived by basic impedance theory instead of complicated analytical derivation as given in [11], [13], and [14]. In this paper, all the L-network-cascaded topologies can be generated for LI, CI and ZPA operation (refer to Fig. 4). However, it cannot directly deal with the topologies including non-L-type networks, such as the Lattice network.

A practical application should choose suitable topology based on its terminal condition. For example, the battery charger can use VI topologies if the input is a dc source and the output is directly connected to the battery. If a frond-end dc/dc converter is added at the TX side, then both VI and II topologies are available. From a system perspective, the proposed synthesis method offers a vast potential configurations with good controllability.

V. PRACTICAL DESIGN CONSIDERATION

A. Influence of ESRs

In a high-order resonant tank, all the resonant components have ESRs, and all these ESRs introduce additional conduction losses and affect the transfer function. The quality factor of TX/RX coil are defined as $Q_{tx} (= \omega_s L_{tx}/r_{tx})$ and $Q_{rx} (= \omega_s L_{rx}/r_{rx})$, which are usually much smaller than that of the compensation components. Therefore, the whole resonant tank can be roughly decomposed as two lossless tanks (Tanks TX and RX) and a pair of induced voltage sources with internal resistance (i.e., r_{tx} and r_{rx}) (refer to Fig. 10). Since the ZPA operation is achieved, all the port impedances are resistive. The efficiency for both sides and the whole tank are easily

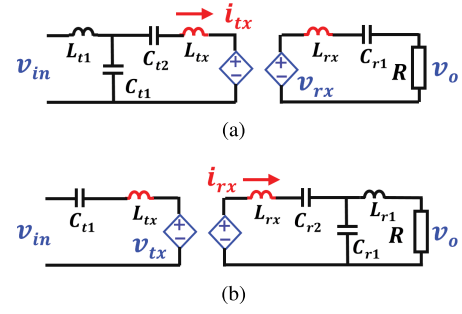


Fig. 14. Example V2V topologies. (a) VVA1. (b) VVB1.

derived as

$$\eta_{tx} = Z_{ref}/(Z_{ref} + r_{tx})$$

$$\eta_{rx} = Z_{rx}/(Z_{rx} + r_{rx})$$

$$\eta_{coil} = \eta_{tx} \eta_{rx}. \quad (5)$$

Once the ESRs are considered, the transfer function of the induced source part is slightly different. (3) is modified as

$$G'_{coil,iv} = \frac{v_{rx}}{i_{tx}} \frac{Z_{rx}}{r_{rx} + Z_{rx}} = G_{coil,iv} * \eta_{rx}$$

$$G'_{coil,vi} = \frac{i_{rx}}{v_{tx}} \frac{Z_{tx}}{r_{tx} + Z_{tx}} = G_{coil,vi} * \eta_{tx}. \quad (6)$$

For topologies of Family A, the accuracy of the transfer function is only determined by η_{rx} , while η_{tx} affects the transfer function of Family B topologies. In this paper, a practical application should properly select and design the topology to minimize the influence of ESRs.

B. Family A Versus Family B

Two V2V topologies are selected to study the difference between Families A and B. The ESR of the coupling coils will not only affect the accuracy of the transfer function, but also leads to different efficiency characteristics for different families. As shown in Fig. 14, the example topologies are generated by VVA and VVB by adding one more capacitor (refer to Fig. 9). Without this capacitor, in practice, it is very difficult to make $L_{tx} = L_{t1}$ for VVA due to the fabrication. Besides, this additional capacitor helps to modify the gain.

According to the impedance requirements for LI output and ZPA operation, the compensation components should be designed according to Table I and Fig. 11. For the TX side of VVA1, LI $G_{tx,vi}$ is ensured by

$$j\omega_s L_{t1} + \frac{1}{j\omega_s C_{t1}} = 0. \quad (7)$$

The resistance transformation of TX side requires

$$j\omega_s L_{t1} = -\frac{1}{j\omega_s C_{t1}} = j\omega_s L_{tx} + \frac{1}{j\omega_s C_{t2}}. \quad (8)$$

For the RX side, the LI $G_{rx,vv}$ and resistance transformation can be fulfilled simultaneously by

$$j\omega_s L_{rx} + \frac{1}{j\omega_s C_{r1}} = 0. \quad (9)$$

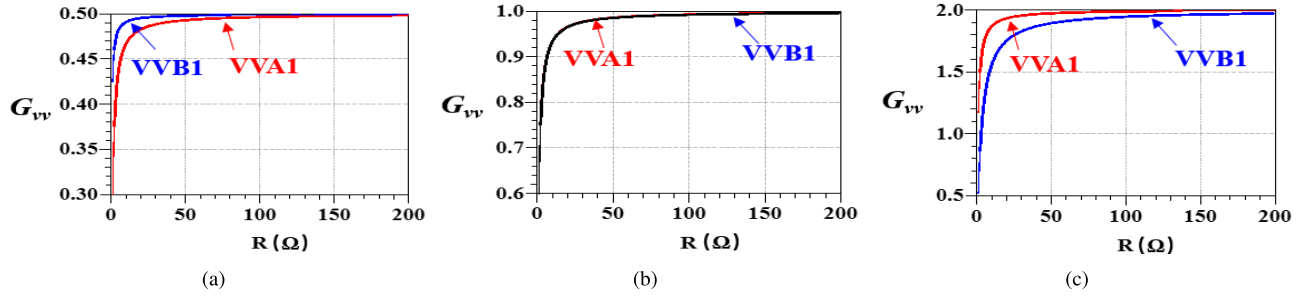


Fig. 15. G_{vv} comparison between VVA1 and VVB1 for different G_{ideal} . (a) $G_{ideal} = 0.5$. (b) $G_{ideal} = 1$. (c) $G_{ideal} = 2$.

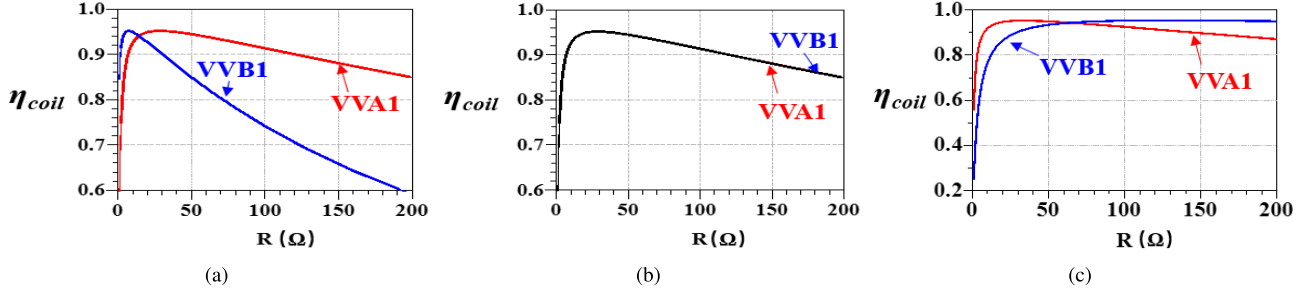


Fig. 16. η_{coil} comparison between VVA1 and VVB1 for different G_{ideal} . (a) $G_{ideal} = 0.5$. (b) $G_{ideal} = 1$. (c) $G_{ideal} = 2$.

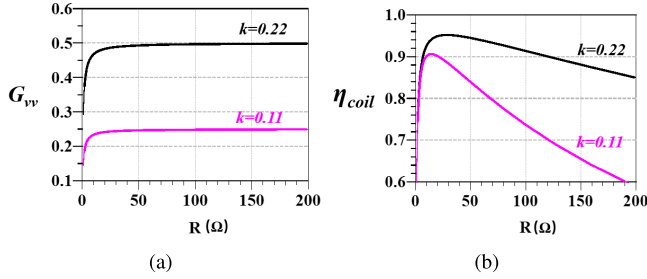


Fig. 17. G_{vv} and η_{coil} of VVA1 when k decreases. (a) G_{vv} . (b) η_{coil} .

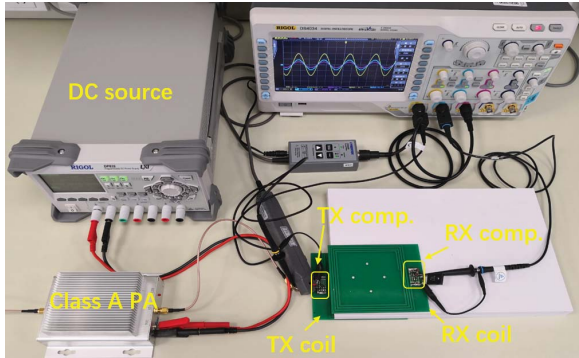


Fig. 18. Experiment setup.

Defining $m_t = L_{t1}/L_{tx}$, the transfer function is then derived as

$$\begin{aligned}
 G_{tx,vi} &= \frac{1}{jm_t\omega_s L_{tx}} \\
 G_{coil,iv} &= j\omega_s k \sqrt{L_{tx} L_{rx}} \\
 G_{rx,vv} &= 1 \\
 G_{vv} &= G_{tx,vi} G_{coil,iv} G_{rx,vv} = \frac{k}{m_t} \sqrt{\frac{L_{rx}}{L_{tx}}}. \quad (10)
 \end{aligned}$$

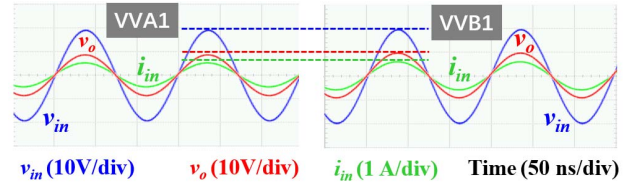


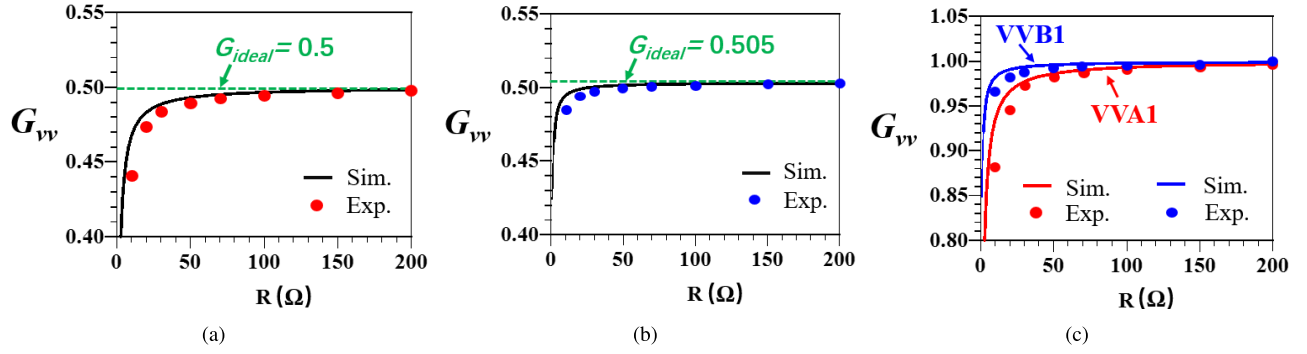
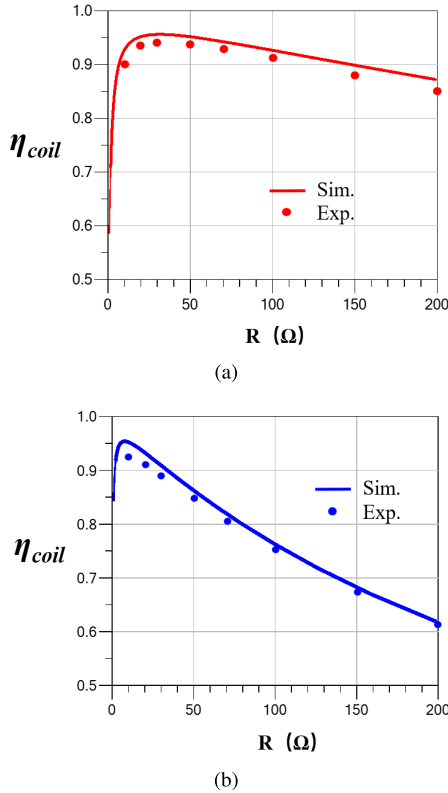
Fig. 19. Full-load waveforms of VVA1 and VVB1.

Similarly, the impedance requirement and the transfer function for VVB1 are derived as follows:

$$\begin{aligned}
 j\omega_s L_{tx} + \frac{1}{j\omega_s C_{r1}} &= 0 \\
 j\omega_s L_{r1} + \frac{1}{j\omega_s C_{r1}} &= 0 \\
 j\omega_s L_{r1} &= j\omega_s L_{rx} + \frac{1}{j\omega_s C_{r2}} \\
 m_r &= L_{r1}/L_{rx} \\
 G_{vv} &= \frac{m_r}{k} \sqrt{\frac{L_{rx}}{L_{tx}}}. \quad (11)
 \end{aligned}$$

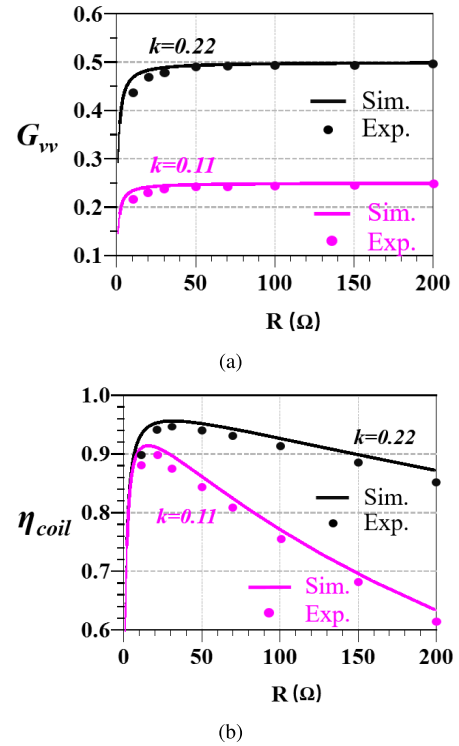
For a specific application, the power level and output voltage together determine the range of R , i.e., from full load ($R = R_{min}$) to light load ($R = +\infty$). In this paper, both VVA1 and VVB1 can be properly designed for a target voltage gain, G_{ideal} . A simulation is built based on Table II, and all the other resonant components are designed according to (7)-(11). For different G_{ideal} in Fig. 15, there is an error between G_{vv} and G_{ideal} due to the coils' ESRs. Heavier load causes larger error.

According to (6), the real gain of Family A topologies is only affected by η_{tx} . Since VVA1 uses series compensation at the RX side, all the G_{vv} curves are exactly the same in Fig. 15. In a different manner, the real gain of Family-B topologies is

Fig. 20. G_{vv} comparison. (a) VVA1. (b) VVB1. (c) VVA1 versus VVB1: r .Fig. 21. η_{coil} comparison. (a) VVA1. (b) VVB1.

affected by η_{tx} , which means G_{vv} of VVB1 is dependent on both-side ESRs. Therefore, the G_{vv} curves of VVB1 are quite different in Fig. 15 for different G_{ideal} . Usually a low-cost and simple IPT system may prefer working in an open-loop manner, and no other switch-mode circuits are used. For this case, VVB1 is better than VVA1 when $G_{ideal} < 1$. When $G_{ideal} = 1$, both topologies have the same error due to the circuit duality. If $G_{ideal} > 1$, VVA1 works better. It should be noted that all the discussion above is valid for fixed or roughly fixed coupling case. If an IPT system has a large coupling variation or wants to achieve accurate G_{vv} , additional dc/dc converters are still required, as such a frond-end state at the TX side.

For high-power applications, η_{coil} has to be considered when selecting the topology. For VVA1, the coil efficiency defined

Fig. 22. Influence of decreased k . (a) G_{vv} . (b) η_{coil} .

by (5) can be further derived as

$$\eta_{coil} = \frac{\omega^2 L_{tx} L_{rx}}{\omega^2 L_{tx} L_{rx} + r_{tx}(R + r_{tx})} * \frac{R}{R + r_{tx}} \quad (12)$$

which is independent on G_{ideal} . However, the case for VVB1 is quite different. The final load R is inverted by the secondary side compensation. The coil efficiency is derived as

$$\eta_{coil} = \frac{\omega^2 L_{tx} L_{rx}}{\omega^2 L_{tx} L_{rx} + r_{tx} \left(\frac{X^2}{R} + r_{tx} \right)} * \frac{\frac{X^2}{R}}{\frac{X^2}{R} + r_{tx}} \quad (13)$$

where $X = \omega k \sqrt{L_{tx} L_{rx}} G_{ideal}$. This efficiency depends on G_{ideal} . Fig. 16 compares η_{coil} for different G_{ideal} . If $G_{ideal} < 1$, VVB1 works better than VVA1 for heavy load condition, but its efficiency drops much faster than that of VVA1 when the load becomes lighter [refer to Fig. 16(a)]. However, the conclusion is reversed when $G_{ideal} > 1$ [refer to Fig. 16(c)].

TABLE II
COIL PARAMETERS

f_s	L_{tx} & L_{rx}	Q_{tx} & Q_{rx}	k
6.78 MHz	3.34 μH	200	0.22

When k drops due to the position change, v_{in} should be used to compensate the decreased G_{VV} for constant v_o [refer to (10)]. Here VVA1 with $G_{ideal} < 1$ is used as a study case because it shows good efficiency for a wide load range [refer to Fig. 16(a)]. As shown in Fig. 17, G_{VV} is linearly proportional to k , and decreased k directly leads to an efficiency drop.

C. Experimental Verification

The final experiment setup is shown in Fig. 18. A Class-A power amplifier (PA) is used to drive the high-order-compensated coils. This linear PA can provide a pure sinusoidal driving voltage. The coils' parameters are given in Table II. High- Q capacitors (about 2000) and inductors (about 800) are used for compensation. A 6.78-MHz IPT system is built with $k = 0.22$, $v_{in} = 20$ V, and $R_{min} = 10 \Omega$. It is hard to exactly achieve the same G_{ideal} for VVA1 and VVB1 under fixed k , because it is impossible to continuously tune the compensation inductors (refer to L_{t1} and L_{r1} in Fig. 14). In the experiment, the $G_{ideal} < 1$ case is studied. L_{t1} of VVA1 is tuned at 1.47 μH to provide $G_{ideal} = 0.5$; L_{r1} of VVB1 is tuned at 0.35 μH to have $G_{ideal} = 0.505$.

First of all, both VVA1 and VVB1 are built to verify the ZPA operation. The waveforms of v_{in} , v_o , and i_{in} are measured for full-load condition as shown in Fig. 19. It clearly shows v_{in} is in phase with i_{in} , and ZPA is achieved for both topologies. v_o is also in phase with v_{in} as predicted by (10) and (11).

The measured G_{VV} is compared with the simulation in Fig. 20(a) and (b). For both topologies, the measured G_{VV} are well-matched with the simulation results. In order to compare VVA1 and VVB1, the ratio between the achieved G_{VV} and the target gain G_{ideal} is defined as $r = G_{VV}/G_{ideal}$. Then, the results of Fig. 20(a) and (b) can be converted and compared in Fig. 20(c). The difference between VVA1 and VVB1 validates that VVB1 has smaller error than VVA1 [refer to Fig. 15(a)]. The measured η_{coil} are compared in Fig. 21. A good consistency is also observed between the experiment and the simulation. The small error is mainly caused by the ESRs of other resonant components. The peak efficiencies for both topologies are all above 93%.

When k drops, the input source is tuned to ensure a constant output voltage. In this case, v_o is maintained at 10 V by manually fine tuning v_{in} . Fig. 22 compares the measured G_{VV} and η_{coil} with the simulation results for different coupling conditions. When k drops from 0.22 to 0.11, the measured G_{VV} also drops as the simulation predicts. Besides, the measured η_{coil} are also well consistent with the simulation results, and the efficiency drop is observed due to the drop of k .

VI. CONCLUSION

A novel and simple system deposition and synthesis method is proposed in this paper for IPT systems. The induced voltage

source model is effectively employed to fully utilize the LI transfer functions between the coupling coils. The self-inductances are aborted by both-side compensations. Using this modeling approach, the high-order IPT resonant tank is no longer treated as an entity and is effectively decomposed as three parts. This paper modifies the mature topology synthesis method for the conventional resonant converter and applies this method for IPT compensation synthesis. The tank candidates are generated to achieve coupling-independent resonance, loading-independent output, and ZPA operation. Many novel topologies are developed for four kinds of conversion. Based on the coil transfer function, two families of IPT topologies are proposed and compared. Besides, the proposed modeling method can easily deal with the coil ESRs, and it shows that the actual transfer function and efficiency of two families of topologies are affected by the coil ESR in a quite different manner. Finally, the experimental results well explain the influence of ESRs on the two-family topologies. The proposed method dramatically simplifies the selection, analysis, and design of high-order-compensated IPT systems.

REFERENCES

- [1] N. B. Carvalho *et al.*, "Wireless power transmission: R&D activities within Europe," *IEEE Trans. Microw. Theory Techn.*, vol. 62, no. 4, pp. 1031–1045, Apr. 2014.
- [2] M. Fu, T. Zhang, C. Ma, and X. Zhu, "Efficiency and optimal loads analysis for multiple-receiver wireless power transfer systems," *IEEE Trans. Microw. Theory Techn.*, vol. 63, no. 3, pp. 801–812, Mar. 2015.
- [3] Z. Liu, Z. Zhong, and Y. Guo, "In vivo high-efficiency wireless power transfer with multisine excitation," *IEEE Trans. Microw. Theory Techn.*, vol. 65, no. 9, pp. 3530–3540, Sep. 2017.
- [4] M. Fu, H. Yin, and C. Ma, "Megahertz multiple-receiver wireless power transfer systems with power flow management and maximum efficiency point tracking," *IEEE Trans. Microw. Theory Techn.*, vol. 65, no. 11, pp. 4285–4293, Nov. 2017.
- [5] A. Pacini, A. Costanzo, S. Aldhaher, and P. D. Mitcheson, "Load- and position-independent moving MHz WPT system based on GaN-distributed current sources," *IEEE Trans. Microw. Theory Techn.*, vol. 65, no. 12, pp. 5367–5376, Dec. 2017.
- [6] C.-S. Wang, G. A. Covic, and O. H. Stielau, "Power transfer capability and bifurcation phenomena of loosely coupled inductive power transfer systems," *IEEE Trans. Ind. Electron.*, vol. 51, no. 1, pp. 148–157, Feb. 2004.
- [7] C.-S. Wang, O. H. Stielau, and G. A. Covic, "Design considerations for a contactless electric vehicle battery charger," *IEEE Trans. Ind. Electron.*, vol. 52, no. 5, pp. 1308–1314, Oct. 2005.
- [8] T. C. Beh, M. Kato, T. Imura, S. Oh, and Y. Hori, "Automated impedance matching system for robust wireless power transfer via magnetic resonance coupling," *IEEE Trans. Ind. Electron.*, vol. 60, no. 9, pp. 3689–3698, Sep. 2013.
- [9] M. Fu, C. Ma, and X. Zhu, "A cascaded boost-buck converter for high efficiency wireless power transfer systems," *IEEE Trans. Ind. Inform.*, vol. 10, no. 3, pp. 1972–1980, Jul. 2015.
- [10] M. Fu, H. Yin, M. Liu, Y. Wang, and C. Ma, "A 6.78 MHz multiple-receiver wireless power transfer system with constant output voltage and optimum efficiency," *IEEE Trans. Power Electron.*, vol. 33, no. 6, pp. 5330–5340, Jun. 2018.
- [11] W. Zhang, S.-C. Wong, C. K. Tse, and Q. Chen, "Design for efficiency optimization and voltage controllability of series-series compensated inductive power transfer systems," *IEEE Trans. Power Electron.*, vol. 29, no. 1, pp. 191–200, Jan. 2014.
- [12] Y. H. Sohn, B. H. Choi, E. S. Lee, G. C. Lim, G. H. Cho, and C. T. Rim, "General unified analyses of two-capacitor inductive power transfer systems: Equivalence of current-source SS and SP compensations," *IEEE Trans. Power Electron.*, vol. 30, no. 11, pp. 6030–6045, Nov. 2015.
- [13] X. Qu, W. Zhang, S.-C. Wong, and C. K. Tse, "Design of a current-source-output inductive power transfer LED lighting system," *IEEE J. Emerg. Sel. Topics Power Electron.*, vol. 3, no. 1, pp. 306–314, Mar. 2015.

- [14] A. Costanzo *et al.*, "Conditions for a load-independent operating regime in resonant inductive WPT," *IEEE Trans. Microw. Theory Techn.*, vol. 65, no. 4, pp. 1066–1076, Apr. 2017.
- [15] G. A. Covic, J. T. Boys, M. L. G. Kissin, and H. G. Lu, "A three-phase inductive power transfer system for roadway-powered vehicles," *IEEE Trans. Ind. Electron.*, vol. 54, no. 6, pp. 3370–3378, Dec. 2007.
- [16] Z. Pantic, S. Bai, and S. M. Lukic, "ZCS LCC-compensated resonant inverter for inductive-power-transfer application," *IEEE Trans. Ind. Electron.*, vol. 58, no. 5, pp. 3500–3510, Aug. 2011.
- [17] S. Li, W. Li, J. Deng, T. D. Nguyen, and C. C. Mi, "A double-sided LCC compensation network and its tuning method for wireless power transfer," *IEEE Trans. Veh. Technol.*, vol. 64, no. 6, pp. 2261–2273, Jun. 2015.
- [18] W. Zhang and C. C. Mi, "Compensation topologies of high-power wireless power transfer systems," *IEEE Trans. Veh. Technol.*, vol. 65, no. 6, pp. 4768–4778, Jun. 2016.
- [19] X. Qu, Y. Jing, H. Han, S.-C. Wong, and C. K. Tse, "Higher order compensation for inductive-power-transfer converters with constant-voltage or constant-current output combating transformer parameter constraints," *IEEE Trans. Power Electron.*, vol. 32, no. 1, pp. 394–405, Jan. 2017.
- [20] J. Lu, G. Zhu, D. Lin, S.-C. Wong, and J. Jiang, "Load-independent voltage and current transfer characteristics of high-order resonant network in IPT system," *IEEE Trans. Emerg. Sel. Topics Power Electron.*, vol. 7, no. 1, pp. 422–436, Mar. 2018.
- [21] J. Hou, Q. Chen, Z. Zhang, S.-C. Wong, and K. T. Chi, "Analysis of output current characteristics for higher order primary compensation in inductive power transfer systems," *IEEE Trans. Power Electron.*, vol. 33, no. 8, pp. 6807–6821, Aug. 2018.
- [22] I. Batarseh, "Resonant converter topologies with three and four energy storage elements," *IEEE Trans. Power Electron.*, vol. 9, no. 1, pp. 64–73, Jan. 1994.



Rong He (S'19) was born in Hengyang, Hunan, China, in 1996. She received the B.S. degree in electrical engineering and automation from the Harbin Institute of Technology, Weihai, China, in 2018. She is currently pursuing the M.S. degree in power electronics at the School of Information Science and Technology, ShanghaiTech University, Shanghai, China.

In September 2018, she joined the Advanced Electronic Power Conversion Laboratory, School of Information Science and Technology, ShanghaiTech University. Her current research interests include the compensation network of the inductive power transfer (IPT) system and multiple-coil IPT systems.



Peng Zhao (S'19) was born in Luan, Anhui, China, in 1995. He received the B.S. degree in electrical engineering from the Hefei University of Technology, Hefei, China, in 2017. He is currently pursuing the M.S. degree in power electronics from ShanghaiTech University, Shanghai, China.

His current research interests include the small and medium power application of the inductive power transfer system and resonant converters.



Minfan Fu (S'13–M'16) received the B.S., M.S., and Ph.D. degrees in electrical and computer engineering from the University of Michigan–Shanghai Jiao Tong University Joint Institute, Shanghai Jiao Tong University, Shanghai, China, in 2010, 2013, and 2016, respectively.

From 2016 to 2018, he held a post-doctoral position with the Center for Power Electronics Systems, Virginia Polytechnic Institute and State University, Blacksburg, VA, USA. He is currently an Assistant Professor with the School of Information Science and Technology, ShanghaiTech University, Shanghai. His current research interests include megahertz wireless power transfer, high-frequency power conversion, high-frequency magnetic design, and application of wide bandgap devices.



Yu Liu (S'13–M'17) received the B.S. and M.S. degrees in electrical engineering from Shanghai Jiao Tong University, Shanghai, China, in 2011 and 2013, respectively, and the M.S. and Ph.D. degrees in electrical engineering from the Georgia Institute of Technology, Atlanta, GA, USA, in 2013 and 2017, respectively.

He is currently a Tenure-Track Assistant Professor with the School of Information Science and Technology, ShanghaiTech University, Shanghai. His current research interests include modeling, protection, fault location, and state/parameter estimation of power systems and power electronic systems.



Haoyu Wang (S'12–M'14–SM'18) received the bachelor's degree (Hons.) in electrical engineering from Zhejiang University, Hangzhou, China, and the master's and Ph.D. degrees in electrical engineering from the University of Maryland at College Park, College Park, MD, USA.

He is currently a Tenure-Track Assistant Professor with the School of Information Science and Technology at ShanghaiTech University, Shanghai, China. His current research interests include power electronics, plug-in electric and hybrid electric vehicles, the applications of wide bandgap semiconductors, renewable energy harvesting, and power management integrated circuits.

Dr. Wang is an Associate Editor of the *IEEE TRANSACTIONS ON TRANSPORTATION ELECTRIFICATION* and an Associate Editor of the *CPSS Transactions on Power Electronics and Applications*.



Junrui Liang (S'09–M'10) received the B.E. and M.E. degrees in instrumentation engineering from Shanghai Jiao Tong University, Shanghai, China, respectively, and the Ph.D. degree in mechanical and automation engineering from The Chinese University of Hong Kong, Hong Kong, in 2010.

Since 2013, he has been an Assistant Professor with the School of Information Science and Technology, ShanghaiTech University, Shanghai. His current research interests include energy conversion and power conditioning circuits, kinetic energy harvesting and vibration suppression, mechatronics, and IoT devices. He has filed two Chinese patents. His research has led to publications including more than 50 technical papers in international journals and conference proceedings.

Dr. Liang serves as a member in the Technical Committee of Power and Energy Circuits and Systems of the IEEE Circuits and Systems Society and the Energy Harvesting Technical Committee in Adaptive Structures and Material Systems Branch, ASME Aerospace Division. He has also served as a Program Committee member of the SPIE Smart Structures + Nondestructive Evaluation Conference. He was a recipient of one Best Student Contributions Award of the 19th International Conference on Adaptive Structures and Technologies, two Best Paper Awards of the IEEE International Conference on Information and Automation, the Postgraduate Research Output Award from The Chinese University of Hong Kong, and the Excellent Research Award 2018 from ShanghaiTech University. He is an Associate Editor of *IET Circuits, Devices and Systems* and the General Chair of the 2nd International Conference on Vibration and Energy Harvesting Applications.